Chemical Science

Accepted Manuscript

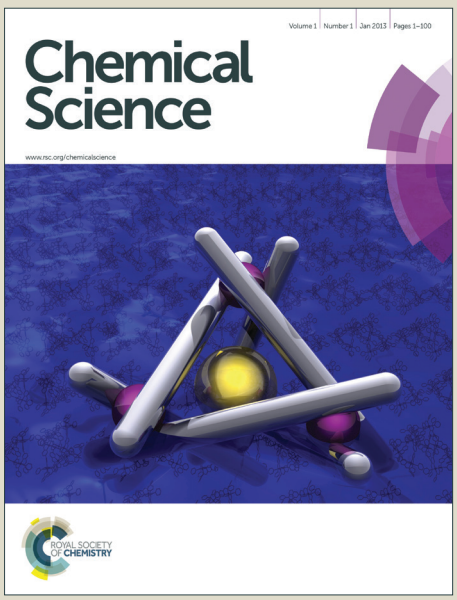

ROYAL SOCIETY OF CHEMISTRY

www.rsc.org/chemicalscience

Tissue Distribution and Urinary Excretion of Intravenously Administered Chemically Functionalized Graphene Oxide Sheets

Dhifaf A. Jasim[a,^], Cécilia Ménard-Moyon[b,^] Dominique Bégin[c], Alberto Bianco[b,], Kostas Kostarelos[a,*]*

[a] *Nanomedicine Laboratory, Faculty of Medical & Human Sciences and National Graphene Institute, University of Manchester, AV Hill Building, Manchester M13 9PT, United Kingdom*

[b] *CNRS, Institut de Biologie Moléculaire et Cellulaire, Laboratoire d'Immunopathologie et Chimie Thérapeutique, 67000 Strasbourg, France*

[c] *Institut de Chimie et Procédés pour l'Energie, l'Environnement et la Santé (ICPEES), ECPM, UMR 7515 du CNRS, University of Strasbourg, 25 rue Becquerel Cedex 02, 67087 Strasbourg, France.*

^ These authors contributed equally to this work.

** Correspondence to either: a.bianco@ibmc-cnrs.unistra.fr; kostas.kostarelos@manchester.ac.uk*

Abstract

Design of graphene-based materials for biomedical purposes is of great interest. Graphene oxide (GO) sheets represent the most widespread type of graphene materials in biological investigations. In this work, thin GO sheets were synthesized and further chemically functionalized with DOTA (1,4,7,10-tetraazacyclododecane-1,4,7,10-tetraacetic acid), a stable radiometal chelating agent, by an epoxide opening reaction. We report the tissue distribution of the functionalized GO sheets labelled with radioactive indium (^{111}In) after intravenous administration in mice. Whole body single photon emission computed tomography (SPECT/CT) imaging, gamma counting studies, Raman microscopy and histological investigations indicated extensive urinary excretion and predominantly spleen accumulation. Intact GO sheets were detected in the urine of injected mice by Raman spectroscopy, high resolution transmission electron microscopy (HR-TEM) and electron diffraction. These results offer a previously unavailable pharmacological understanding on how chemically functionalized GO sheets transport in the blood stream and interact with physiological barriers that will determine their body excretion and tissue accumulation.

Keywords: Graphene, Toxicity, Biodistribution, Pharmacokinetics, Pharmacology

Introduction

Graphene and related materials exhibit outstanding properties generated from their unique 2D carbon geometry (1, 2). These properties have attracted great interest by different scientific disciplines, ranging from physics, materials science and more recently biomedicine (2-5). One of the most interesting properties for biomedical applications is their large available surface area that provides an ideal platform for bio-functionalization with small therapeutic molecules, macromolecules and imaging probes by covalent attachment or physisorption (6-8). The high mechanical strength (9-11) and flexibility of graphene material (2, 3) offer interesting and largely unexplored possibilities on interaction with soft biological matter (10, 12) some of which directly relevant to regenerative medicine and prosthetic applications (2).

Graphene oxide (GO) is only one type in the graphene family nanomaterials (13, 14). Even though it suffers from compromised electronic properties due to the extensive surface defects caused by oxidation (7, 15) it has been extensively explored in the biological context. The availability of several types of oxygenated groups on the edge and planar surface of GO facilitates dispersibility and stability in physiological environments that affords improved biocompatibility (6).

In view of the potential in using graphene materials for biomedical applications, it is critical to understand its interaction and fate *in vivo* (16). GO prepared by the modified Hummers' method has been administered intravenously (17-19), intraperitoneally (20, 21), orally (21) and intravitreally (22) with no reported cytotoxic responses, histopathological changes or inflammatory reaction, even after long exposure time points (21, 22). After intravenous or intraperitoneal administration, GO has been reported to accumulate mainly in the reticuloendothelial system (RES) organs with slow clearance over time (17, 23). Direct lung administration by intratracheal, intrapleural or pharyngeal aspiration of pristine graphene, GO or reduced GO (rGO) resulted in lung retention with activation of the acute and chronic inflammatory pathways and lung injury (24-26). However, no biopersistance was seen with slow clearance in the mediastinal lymph nodes over time (25). Moreover, *in vivo* degradation of intravenously injected functionalized graphene three months post-injection has been reported in tissue residing macrophages, mainly in the spleen (27).

It must be emphasized that all above mentioned studies have used different types of GO (14, 28) that can result in sharply different biological interactions (29, 30). These interactions will be dependent on the type of surface functionalization, functional surface groups (31, 32) and dimensions of the GO sheets (17). Here, we report whole body imaging and pharmacokinetic data following intravenous administration of DOTA-

functionalized GO (GO-DOTA) coupled with analytical and histopathological analysis of critical organs using individualized stable dispersions of thin GO sheets.

Results

Preparation and Characterization of GO and GO-DOTA. GO was prepared by the modified Hummers' method as described previously (20). To allow the grafting of DOTA, GO was initially derivatized with amine functions (**Scheme 1**). For this purpose, we exploited the presence of epoxy functions on the basal plane of GO (33) which are highly reactive towards nucleophiles (34, 35). We used triethylene glycol (TEG) diamine to open the epoxy rings and introduce amino functions on GO. The TEG chain preserved aqueous dispersibility of GO. The amount of amino groups on GO-NH_2 was assessed by the Kaiser test (36). The loading corresponded to 670 µmol of NH_2 functions per gram of GO. Then, the amino groups of GO-NH_2 were derivatized with a DOTA derivative bearing an isothiocyanate moiety (DOTA-NCS). Kaiser test of GO-DOTA indicated that the amount of unreacted amine functions was 315 µmol/g, accounting for a ~50% coupling efficiency.

Structural characterization of both GO-NH_2 and GO-DOTA are shown in **Figure 1** using transmission electron microscopy (TEM) and atomic force microscopy (AFM). The AFM height sections (**Figure 1A** and **S1)** revealed that the thickness of the GO sheets was increased from single to few layers after functionalization, while the size distribution was moderately reduced. DOTA conjugation onto GO was further studied by Fourier transform infrared (FT-IR) spectroscopy, X-ray photoelectron spectroscopy (XPS), thermogravimetric analysis (TGA) and Raman spectroscopy (**Figures 1B** and **S2)**. The appearance of new bands in the FT-IR spectra of GO-NH_2 and GO-DOTA evidenced the chemical modification of GO. XPS confirmed the presence of nitrogen after derivatization with TEG diamine and DOTA-NCS. TGA under inert atmosphere allowed to determine the thermal profile of GO and functionalized GO as the functional groups on the graphene surface are thermally labile. The different changes observed were indicative of covalent functionalization of GO. The I_D/I_G ratio of GO derivatives obtained from the Raman spectra were increased in comparison to the starting graphite, as the samples were covalently functionalized.

Radiolabeling Efficiency and Stability of GO-DOTA[^{111}In]. The efficiency of radiolabeling GO-DOTA was compared to a physically adsorbed control (GO + DOTA), prepared by simple mixing GO with DOTA (**Scheme S1**), and to controls (DOTA[^{111}In] and

EDTA[^{111}In]). As shown in **Figure S3 A**, the radiolabeling efficiency of the covalent sample was found double that of the physically adsorbed control. Removal of unbound DOTA[^{111}In] and EDTA[^{111}In] was performed by centrifugation and no free ^{111}In label or DOTA were detected in the covalent sample as displayed in **Figure S3 B**. This was also confirmed before injecting the samples into C57BL/6 mice (**Figure S3 C**). DOTA conjugation efficiency was further analysed using a modified running buffer at high pH (pH 9). At this pH, free ^{111}In precipitates at the application point, while any chelator (DOTA) bound ^{111}In runs to the solvent front. **Figure S3 D** revealed no free DOTA chelator in the sample, confirming further DOTA conjugation.

The radiolabelling stability of GO-DOTA[^{111}In] and GO + DOTA[^{111}In] in both 50% serum and PBS at 37^{0}C up to 24h are shown in **Figure S3 E.** The physically adsorbed sample (GO + DOTA) showed release of DOTA over time, with 50% release in serum, while the covalent sample was stable up to 24 h. Similar results were obtained when simply mixing GO with ^{111}In the absence of DOTA, where the labelling was both unstable and non-efficient (data not shown). Furthermore, the colloidal stability of the GO-DOTA was studied in different dispersion media, including dextrose 5%, PBS and 50% serum **(Figure S4)**. GO-DOTA sheet dispersions were very stable in dextrose and serum-containing media, however aggregation and increase in mean particle diameter was detected in the PBS environment very rapidly, suggesting electrostatic destabilisation.

Pharmacokinetics and tissue distribution after i.v. administration. The biodistribution of GO-DOTA[^{111}In] by SPECT/CT imaging and cut-and-count γ-scintigraphy is displayed in **Figure 2A-D**. Rapid clearance from blood was detected within the first hour following administration (**Figure 2C**) with a strong bladder signal, along with spleen and liver uptake (**Figure 2A**). The whole-body SPECT/CT imaging data were validated by counting the percentage of injected dose of GO-DOTA[^{111}In] per gram of tissue measured by gamma scintigraphy in a separate experiment (**Figure 2B**). At 4h post-injection, a stronger signal was detected in the bladder by SPECT/CT, indicating further urinary excretion. This was in agreement with the significant quantity that was detected in the pooled urine samples after 24h (**Figure 2D)** using metabolic cages. Both controls (DOTA[^{111}In] and EDTA[^{111}In] showed almost complete clearance within the first hour, by both SPECT/CT imaging and *γ*-scintigraphy (**Figure S5**).

Translocation of the signal from the liver to spleen was observed between 4h and 24h after administration, with signal accumulation mainly in the spleen after 24h. This was further confirmed using histology H & E (haematoxylin and eosin) staining of paraffin embedded tissue sections and Raman spectroscopy of homogenized tissue samples at different locations (**Figure 3** and **Figure S6**). Neither H & E nor Raman allowed detection

of the material in the lung or kidneys, suggesting no accumulation in these tissues. Furthermore, no organ damage or other structural changes were observed in all examined organs (including lungs and kidneys) at any time point (**Figure S7**).

Urinary excretion and urine analysis. To further examine the extent of urinary excretions of GO-DOTA, urine samples were analyzed by Raman spectroscopy and TEM, as shown in **Figure 4** and **Figure S8**. GO-DOTA sheets were detected in the urine of injected mice by both Raman spectroscopy and HR-TEM. The Raman signature of GO-DOTA was detected in the urine of injected mice as displayed in **Figure 4A,** the D band appeared wider and the I_D/I_G ratio was further increased in the urine samples to 1.55 ± 0.14, however without statistical significance (Student *t*-test) compared to the GO-DOTA before injection. HR-TEM coupled to selected area of electron diffraction (SAED) confirmed the crystalline nature of GO by the observation of the same set of six-fold symmetric diffraction spots at different locations within the samples (the GO in **Figure 4B i** contains a few layers of graphene). When increasing the magnification further, the atomically thin graphene lattice can be resolved at some locations, whereby being defective in others indicating the impact of functionalization on the hexagonal lattice (**Figure 4B vi** and **vii**).

Discussion

The structural characterization of the functionalized GO derivatives by AFM and TEM (**Figure 1** & **S1**) revealed that the GO sheets were increased in thickness following chemical functionalization with the DOTA chelator. This pattern has been previously reported by others after functionalization of GO with different moieties like polyethylene glycol (PEG) (21, 37), dextran (38) and bovine serum albumin (39). Surface functionalization of GO has also been reported to reduce the lateral dimension of the sheets (39), also in agreement with our data (**Figure S1 ii**). The presence of physically adsorbed water intercalated between GO layers makes the interpretation of the FT-IR analysis difficult and may lead to controversial assignment due to overlapping bands (**Figure 1B i**). The spectrum of GO features 4 main bands: i) a broad band centred at 3400 cm^{-1} corresponding to O-H stretching vibrations of adsorbed water and hydroxyl functions of GO; ii) a band at 1729 cm^{-1} attributed to C=O stretching of carbonyl and carboxyl groups; iii) a band at 1624 cm^{-1} related mainly to H-O-H bending vibrations of water molecules; and iv) a band at 1374 cm^{-1} ascribed to bending vibration of the O-H groups of GO (40). After functionalization of GO with TEG diamine and derivatization with DOTA,

significant differences between the samples was evidenced. The band that could be assigned to the C-O-C vibration band of epoxides (at ~ 1225 cm^{-1}) is very small and in a region with many unassigned bands. Therefore, it is difficult to monitor the derivatization of the epoxide rings. However, the appearance of bands at 2850-2970 cm^{-1} in the GO-NH_2 and GO-DOTA spectra, corresponding to the stretching bands of alkyl groups, demonstrate the successful attachment of the molecules.

XPS was used to determine the surface elemental composition of the GO derivatives (**Figure S2**)**.** The nitrogen (1s) peak of GO-NH_2 and GO-DOTA is displayed in **Figure 1B.ii**. The analyses of GO-NH_2 and GO-DOTA confirmed that nitrogen incorporation (peak at ~ 400 eV) had successfully occurred after derivatization of GO with TEG diamine and DOTA-NCS. In order to offer further evidence of the functionalization of GO, we analyzed the different GO derivatives by TGA under an inert atmosphere (**Figure 1B.iii**). GO is thermally unstable and starts to lose mass at temperatures even lower than 100°C. Below 150°C, the weight loss is attributed to the volatility of water trapped between the GO layers. The higher weight loss at 230°C is due to the elimination of labile oxygen-containing groups (41). The thermal profile of GO after derivatization with TEG diamine is different. The two weight loss slopes at 190 and 350°C can be ascribed to both the elimination of oxygenated moieties and the organic functional groups arising from the newly formed carbon-bound TEG. As the thermal decomposition of TEG diamine takes place at a temperature below 200°C, the higher degradation temperature of GO-NH_2 is a proof of covalent bonding onto GO. Compared with the curve of GO-NH_2, the weight loss of GO-DOTA at the end of the TG analysis (900°C) is significantly higher. Furthermore, the thermal profile of GO-DOTA is different with a lower weight loss below 150°C, revealing a lower amount of stacked water. This change was accompanied by a new thermal decomposition at 565°C, which is proposed to arise from the grafted DOTA moiety, whereas the thermal decomposition of DOTA-NCS occurs at a lower temperature. As shown in the Raman spectra in **Figure 1B.iv**, the I_D/I_G ratio of GO increased dramatically compared to graphite due to the oxidative process. After derivatization of GO with the TEG diamine and DOTA-NCS, the I_D/I_G ratio did not change significantly as the reaction conditions did not lead to the introduction of further defects on the GO surface. Taken together, these data illustrate that GO was successfully covalently derivatized.

Radiolabeling of GO (17) and chemically functionalized GO with radioactive iodine (^{125}I) has been previously reported (16, 21, 38). Iodine radiolabeling requires no chelating agent attachment to the graphene material, however the method involves the use of strong oxidizing agents like chloramine T or iodogen. Moreover, such iodinated constructs are notoriously unstable, while the inherent affinity of iodine for the thyroid gland is a misleading limitation to the biodistribution profiles obtained (38). Radiolabeling with ^{111}In

has been performed previously using physical adsorption of the DTPA (diethylenetriaminepentaacetic acid) chelating agent on the surface of GO by π-stacking. Such strategy however is prone to disproportion; the thickness of the GO sheets used was exceedingly large (42), which suggests it is within the ultrafine graphite category rather than the graphene category (14).

Investigation of the radiolabeling efficiency and stability of GO-DOTA[^{111}In] confirmed the successful covalent conjugation of DOTA on the surface of GO, and ensured that the labeling was suitable and stable in biological media for the subsequent biodistribution studies. The radiolabeling efficiency of GO-DOTA[^{111}In] was found to be more than double the efficiency of the physically adsorbed control (GO + DOTA[^{111}In]) (**Figure S3 A)**. GO-DOTA[^{111}In] was stable overtime up to 24 h at 37^{0}C, while, the labeled fraction of the mixed control showed no stability over time with more than 50% release after 24 h in serum (**Figure S3 A, B,** and **E**). All non-chelated ^{111}In was removed by centrifugation until no free ^{111}In signal was obtained in the samples before injection (**Figure S3 B** and **C**). The high stability of the radiolabeled material in serum, together with the sharply different tissue distribution profiles for both control samples compared to GO-DOTA[^{111}In], were considered indicative of efficient GO labeling that allowed accurate determination of GO-DOTA[^{111}In] biodistribution, with negligible release of ^{111}In label from the conjugate. The aggregation of GO-DOTA sheets detected in PBS was thought to be due to the presence of high salt concentration, while the presence of sugar (in 5% dextrose) and protein (in serum-containing media) molecules afforded greater colloidal stability to the sample **(Figure S4).**

The biodistribution profile of the GO-DOTA[^{111}In] conjugate using SPECT/CT imaging and γ-scintigraphy showed at the early times after intravenous injection, strong signals detected in the bladder and urine of the GO-DOTA[^{111}In] treated mice (**Figure 2**). This profile was different from all animals injected with the controls, where complete clearance within the first hour was observed with minimal bladder residence (**Figure S5**). The urinary excretion of GO material was further confirmed by HR-TEM of the collected urine samples (**Figure 4B** and **S8**) showing hexagonal lattice fringes. The typical GO diffraction patterns from the SAED analysis performed at different locations within the sample showed the expected characteristic six-fold symmetry of the honeycomb organized lattice of graphene sheets at some locations with defective hexagons at others (**Figure 4 vi** and **vii**). The zoomed in images (**Figure 4 vi and vii**) showed some defect-free areas interspersed with defected areas. This has been reported for chemically derived graphene materials that originate from the oxidation-reduction treatment (43).

The Raman signature of GO-DOTA detected in the urine of injected mice further confirmed intact sheet urinary excretion (**Figure 4A)**. The increase in the width of the D

band and ratio of the I_D/I_G bands may be indicative of further defects introduced on the surface of the GO-DOTA[^{111}In] during transport through blood circulation and excretion, however the absence of statistical significance compared to the GO-DOTA before injection warrants the need for work. Increase in I_D/I_G band ratios and widths of D bands of intravenously injected GO has been reported previously in different organs including lung, liver, kidney and spleen starting at 24 h post-injection, but was attributed to biodegradation processes within different tissue-bound macrophages (27).

Previously, only indirect evidence of renal clearance has been reported after intravenous administration of small GO sheets functionalized with dextran (38) or PEG (16, 44). That was due to the reduced dimensions of those sheets that were thought to easily cross the renal filtration slit (< 40 nm) (44, 45). Excretion of GO-DOTA sheets through the renal pathway (**Figure 4** and **S8**) has not been reported before, even though no such GO derivative has been previously synthesized and studied. A possible explanation could be the folding or rolling of the thin sheets into smaller dimensions (46-48) during blood circulation. In this way, a significant fraction of the GO sheets could translocate the glomerular filtration system in a manner similar to that described previously for chemically functionalised single and multi-walled carbon nanotubes (49, 50). Another mechanism could be the sliding of the thin GO sheets perpendicularly through the cellular membranes as suggested *in vitro* (51). Further investigations are certainly warranted to determine the excretion mechanism of such chemically functionalized GO sheets.

Other carbon nanostructures, such as chemically functionalized carbon nanotubes, have been reported to be able to excrete intact in the urine of injected mice (52, 53). Given their average length of 200-500 nm, they were thought to rapidly eliminate through the glomerular filter by alignment with blood flow and perpendicularly translocating through the glomerular filter (49, 54). Hydroxyl-functionalized fullerenes were also reported to be rapidly excreted through the urinary tract of rats and rabbits, while carboxylic acid-functionalized fullerenes were retained mainly in the liver 48 h post-injection (52, 55). It is becoming evident that different carbon nanostructures, with varying dimensions, shape, surface, degree of functionalization and individualization follow different *in vivo* pathways, that determine their tissue affinity, accumulation and excretion (31, 49). We postulate that for graphene material three fundamental parameters are highly important in determining the biological fate. Lateral dimension and thickness (i.e. layer number) may alter the stiffness and flexibility of the material that will have subsequently a great impact on interactions with tissues and cells. Lastly, the degree and nature of the functionalization (the hydrophilic/hydrophobic surface character) of the material (14, 30), that may have an impact on the interactions with proteins of the extracellular matrix or blood plasma.

In this study, GO was observed to translocate from liver to spleen, evidenced by

the reduction of signal in the liver with concomitant increased or persistent signal in the spleen (**Figure 2** and **3**). Tissue distribution of intravenously injected graphene derivatives has been reported previously using material with different surface functionalities. PEG-functionalized GO was reported to accumulate in the RES organs (liver, spleen) with slow clearance over time in urine and faeces, and renal clearance that was attributed to the smaller sized (< 40nm) sheets able to cross the glomerular filtration slit. Accumulation in the RES was attributed to larger sheets uptaken by macrophages, however, no such experimental evidence was shown (16). Another study using both PEG-functionalized GO and rGO constructs, demonstrated maximum organ accumulation in the liver for all constructs, regardless of their significant differences in size and surface characteristics (56). In a different study, high kidney accumulation was reported after 24h from i.v. injected PEG-functionalized small GO (lateral dimension 10-50 nm), with lower accumulation in the lung, liver and spleen (44). In a study using dextran-functionalized GO, mainly liver accumulation in the liver was reported, with both faecal and urinary excretions (38), while NOTA (1,4,7-triazacyclononane-triacetic acid)-functionalized GO-PEG, also shown to accumulate in the liver (57, 58). On the other hand, non-functionalized GO of large lateral dimensions (> 500 nm) administered i.v. in mice has been reported to accumulate to a large extend in the lung (17, 59, 60). However, we speculate that this was mainly due to aggregation among flakes in these GO dispersions. Smaller GO sheets (100-500 nm) were shown to accumulate mainly in the liver (17).

All above studies suggested that dimensions and surface groups are critical to determine the fate of GO after intravenous administration. The two-phase biodistribution profile of the GO sheets studied here can be related to the wide thickness distribution of the GO sheets. We speculate that thin, flexible sheets may tend to roll, fold or slid and cross the glomerular filtration barrier, while thicker sheets may favour entrapment and uptake by spleen cells. The GO-DOTA[^{111}In] construct mainly accumulated in the splenic red pulp (**Figure 3B** and **S6**), that may involve immune cells (e.g. engulfment by spleen-bound macrophages or monocytes) since the splenic red pulp is rich with such cells. The low Raman signal from the faeces samples suggested no involvement of biliary excretion or metabolism by hepatocytes in the time-frame of our experiments.

Our work suggests that further investigations are required to determine the cell types involved in these interactions and whether cellular uptake of the GO sheets occurred by tissue-residing macrophages, or initially by circulating monocytes that subsequently migrate in the spleen. It has been previously reported that medium-sized nanoparticles (10–300nm in diameter) tend to accumulate in the liver and spleen, as these organs contain high numbers of macrophages (61). Such findings have been proposed as a strategy to label and image macrophages in cancer, atherosclerosis, myocardial infarction

and stroke, since macrophage infiltration is involved in all of these pathologies. Splenic drug delivery could be another potential application of these GO constructs with the aim to effectively transport drugs or enzymes to the spleen for potential immunostimulatory interventions (62).

In conclusion, thin GO sheets were successfully conjugated with the DOTA chelator to offer high chemical and radiolabeling stability. Intravenous administration of the moderately thicker GO-DOTA flakes led to rapid and significant urinary excretion followed by gradual accumulation in the spleen. The detection of intact hexagonal lattices in the excreted urine indicated GO clearance that has not been previously reported. These findings provide further understanding of the kinetics and barrier interactions of the thin functionalized GO sheets after intravenous administration in mice. Such findings have important implications in the future design of graphene-based materials for imaging and therapeutic purposes, as well as the determination of their safety profile.

Experimental

Materials. Flake graphite was purchased from Barnwell. All solvents and analytical grade H_2SO_4 were purchased from Fisher Scientific (UK). All other chemicals including $KMnO_4$, $NaNO_3$, H_2O_2, 2,2′-(ethylenedioxy)bis(ethylamine), and DOTA were purchased from Sigma-Aldrich. 2-(4-isothiocyanatobenzyl)-1,4,7,10-tetraazacyclododecane-1,4,7,10-tetraacetic acid (DOTA-NCS) was purchased from Macrocyclics. The filtration and dialysis membranes were purchased from Millipore and Spectrum Laboratories, Inc., respectively.

Chemical Synthesis of Graphene Oxide. GO was prepared by the modified Hummers' method described in Ali-Boucetta *et al.* (20). Briefly 0.4 g of graphite was mixed with 0.2 g of $NaNO_3$, and 9.2 ml of 96% H_2SO_4. $KMnO_4$ (1.2 g) was then added slowly after obtaining a homogenous mixture. Temperature was monitored carefully during the reaction and was kept between 98−100°C. The mixture was further diluted with 50 ml of deionized H_2O and 3% H_2O_2 was added gradually for the reduction of the residual $KMnO_4$, MnO_2 and Mn_2O_7 to soluble $MnSO_4$ salts. The resulting suspension was purified by several centrifugation steps until the pH of the supernatant was around 7 and a viscous orange/brown layer of pure GO appeared on top of the oxidation by-products. This was the fraction of pure GO that was used for later experiments.

Preparation of GO-NH_2 and GO-DOTA. To a solution of GO (17 mg) in deionized water (17 ml) was added triethylene glycol diamine (2,2′-(ethylenedioxy)bis(ethylamine), 350 µl). The reaction mixture was stirred for 3 days. The solution was then filtered on an Omnipore® polytetrafluoroethylene (PTFE) membrane (0.1 µm). The solid was dispersed in DMF, sonicated for 1 min and filtered again. This procedure was repeated with DMF, methanol (twice), and dichloromethane to give GO-NH_2. The solid was dispersed in deionized water and dialyzed against deionized water using a dialysis membrane of MWCO 12-14,000 Da.

To a suspension of GO-NH_2 (14 mg) in deionized water (7 ml) were added sodium bicarbonate (1.2 mg) and DOTA-NCS (5.7 mg). The reaction mixture was stirred for 3 days. The dispersion was then filtered on a PTFE 0.1 µm membrane. The solid was dispersed in DMF, sonicated for 1 min and filtered again. This procedure was repeated with methanol (twice) and dichloromethane. The dispersion was dialyzed against deionized water using a 12-14,000 Da MWCO dialysis membrane.

Preparation of control sample GO + DOTA. To a solution of GO (130 µg) in water (130 µl) was added DOTA (130 µg). The reaction mixture was sonicated for 1 min and stirred for 1 day. The suspension was then dialyzed against deionized water using a 12-14,000 Da MWCO dialysis membrane.

Preparation of ^{111}In labeled GO-DOTA. GO-DOTA was diluted with an equal volume of 0.2 M ammonium acetate buffer pH 5.5, to which 2-20 MBq as $^{111}InCl_3$ was added. The indium was left to react with the GO-DOTA for 60 min at 60°C, after which the reaction was quenched by the addition of 0.1 M EDTA chelating solution.

Radiolabeling Efficiency of GO-DOTA[^{111}In]. To determine the labeling efficiency, aliquots of each final product were diluted five folds in PBS and then 1 µl spotted on silica gel impregnated glass fibre sheets (PALL Life Sciences, UK). The strips were developed with a mobile phase of 50 mM EDTA in 0.1 M ammonium acetate and allowed to dry before analysis. This was then developed and the autoradioactivity quantitatively counted using a Cyclone phosphor detector (Packard Biosciences, UK). The immobile spot on the TLC strips indicated the percentage of radiolabeled GO-DOTA, while free EDTA[^{111}In] or DOTA[^{111}In] were seen as the mobile spots near the solvent front. DOTA conjugation efficiency studies were performed using a modified running buffer containing no EDTA at pH 9, prepared from methanol and ammonia 3.5% solution at a ratio of 1:1 to precipitate any free ^{111}In.

Radiolabeling and Colloidal Stability of GO-DOTA. To determine the stability of the labeled GO-DOTA[^{111}In], aliquots of each final product were diluted five folds either in PBS or mouse serum and then incubated at 37°C over 24 h. At different time-points (0, 1 and 24 h), 1 µl of the aliquots was spotted on silica gel impregnated glass fibre sheets and then developed, and quantified as described above. To determine the colloidal stability of the GO-DOTA flakes, five-fold dilution of the sample was carried out in dextrose 5%, PBS, or serum (50%) and kept at 37°C up to 4h. Dynamic

light scattering (DLS) was performed at (0h,1h and 4h) using the Malvern Zetasizer Nano ZS (UK). Measurements were performed after dilution with water in 1ml final total volume using disposable cuvettes (Sartorius Stedim, Epsom, UK). Default instrument settings and automatic analysis were used for all measurements. Independent triplicate measurements were carried out. It should be noted that DLS is thought to offer an approximate, semi-quantitative determination of the mean particle diameter in the dispersion, but is not the ideal technique for non-spherical particles.

Physicochemical and Structural Characterization Methods. All samples were characterized by TEM using a BioTwin electron microscope (Philips/FEI), Tecnai 12 instrument operated at 120 kV accelerating voltage. One drop of sample was placed on a formvar/carbon coated copper grid. Filter paper was used to remove the excess of material. AFM was carried out using a multimode AFM on the tapping-mode with an J-type scanner, Nanoscope V controller, Nanoscope v8.15 control software (Veeco, Cambridge, UK) and an Olympus high aspect ratio etched silicon probe (OTESPA) with nominal spring constant of 42N/m (Bruker AXS S.A.S, France). Cantilever oscillation varied between 300 and 350 kHz whilst the drive amplitude was determined by the Nanoscope (v8.15) software. Height images were captured at a scan rate of 1.5 Hz. Data was first-order flattened using the Nanoscope software prior to image export. Images were taken in air, by depositing 20 µl of the graphene dispersion on a freshly cleaved mica surface (Agar Scientific, Essex, UK) coated with poly-lysine 0.01% (Sigma) and allowed to adsorb for 30 sec. Excess unbound material was removed by washing with filtered distilled water, and then allowed to dry in air. Size distributions were carried out using ImageJ software, to measure the lateral dimension of individual graphene sheets. Sheet thickness distribution was determined from AFM height sections. Both size and thickness distributions were based on counting more than 100 sheets from several AFM images. The Kaiser test was performed according to a procedure described in (63). Raman spectra of samples were recorded after preparing the aqueous dispersions and drop casting them on glass slides and evaporation of water. Measurements were carried out using a 50x objective at 780 nm laser excitation using a Renishaw micro-Raman spectrometer. Raman spectra were measured at several different locations and three different spectra were collected for each location. FT-IR spectra were measured on a Perkin Elmer Spectrum One ATR-FT-IR spectrometer. TGA was performed using a TGA1 (Mettler Toledo) apparatus from 30°C to 900°C with a ramp of 10°C/min under N_2 using a flow rate of 50 ml/min and platinum pans. XPS analyses were performed with a MULTILAB 2000 (THERMO) spectrometer equipped with an anode using Al Kα radiation (h□ = 1486.6 eV) during 10 min of acquisition in order to achieve a good signal-to-noise ratio. The C (1s) photoelectron binding energy was set at 284.6 ± 0.2 eV relatively to the Fermi level and used as reference for calibrating the other peak positions.

Animal Handling Procedures. Six- to eight-week-old C57BL6 mice were obtained from Harlan (Oxfordshire, UK), allowed to acclimatize for 1 week and were given food and water for the duration of the experiments. All experiments were conducted with prior approval from the UK Home Office.

Single Photon Emission Computed Tomography (SPECT/CT). Mice were anaesthetized by isofluorane inhalation. Each animal was injected via the tail vein injection with 200 µl containing 50 µg of GO-DOTA[^{111}In] labeled with approximately 5-6 MBq. At different time points after injection (t=1,4 and 24 h), mice were imaged using the Nano-SPECT/CT scanner (Bioscan, USA). SPECT images were obtained in 24 projections over 40-60 min using a four-head scanner with 1.4 mm pinhole collimators. CT scans were taken at the end of each SPECT acquisition and all images were reconstructed with MEDISO software (Medical Imaging Systems). Fusion of SPECT and CT images was carried out using the PMOD software.

Gamma Scintigraphy. For more quantitative assessment of tissue biodistribution, a cut and count study was carried out. Mice were anaesthetized by isofluorane inhalation. Each animal was injected via the tail vein injection with 200 µl containing 50 µg of GO-DOTA[^{111}In] containing approximately 1-2 MBq. Mice were sacrificed at 1, 4 and 24 h after injection, and blood and all major organs and tissues were collected including, heart, lungs, liver, spleen, kidneys, muscle, skin and bone. Urine and faeces were pooled and collected after 24 h. Each sample was weighted and counted on a gamma Counter (Perkin Elmer, USA), together with a dilution of the injected dose with dead time limit below 60%. The percentage injected dose per gram tissue was calculated, using four different mice for each time point.

Histological Analysis. Lungs, liver, spleen and kidneys were extracted from mice at different time points (1, 4 and 24 h) and fixed with 4% paraformaldehyde. This was followed by paraffin embedding of sections at known orientations. Sections of 5 µm were stained with hematoxylin and eosin (H&E) and imaged using a LEICA DM 2000 optical microscope equipped with LEICA application suit v3.2.0 software coupled to LEICA DF295 camera.

Purification of Urine Samples. The urine samples were dialyzed against deionized water using a 300 000 MWCO dialysis membrane and then lyophilized.

Raman Microscopy of Tissue and Urine Samples. Tissues were physically homogenized and placed on glass slides. Urine samples were purified as described above and drop-casted and dried on the glass slide. Spectra were measured at several different locations within the tissue and urine samples. An average of three different readings was collected for each location.

High Resolution Transmission Electron Microscopy (HR-TEM) of Urine Samples. HR-TEM and SAED analyses have been performed on a JEOL 2100F TEM/STEM electron microscope operating at 200 kV.

Statistics. Values are mean ± SD (n= 3-4).Statistical significance was evaluated by Student's t-test ($p<0.05$ *).

Acknowledgments

This work was supported by the Centre National de la Recherche Scientifique (CNRS). Caroline Hadad is gratefully acknowledged for help with TGA. We would like to thank Dris Ihiawakrim for fruitful discussions. The authors gratefully acknowledge financial support from EU FP7-ICT-2013-FET-F GRAPHENE Flagship project (no. 604391). We are also very thankful to Mr Peter Walker, Histology Facility, University of Manchester for his advice and assistance in the tissue histology analysis.

References

1. Geim AK (2009) Graphene: Status and Prospects. *Science* 324(5934):1530-1534.
2. Novoselov KS*, et al.* (2012) A roadmap for graphene. *Nature* 490(7419):192-200.
3. Pan Y, Sahoo NG, & Li L (2012) The application of graphene oxide in drug delivery. *Expert Opinion on Drug Delivery* 9(11):1365-1376.
4. Krishna KV, Menard-Moyon C, Verma S, & Bianco A (2013) Graphene-based nanomaterials for nanobiotechnology and biomedical applications. *Nanomedicine* 8(10):1669-1688.
5. Bitounis D, Ali-Boucetta H, Hong BH, Min D-H, & Kostarelos K (2013) Prospects and Challenges of Graphene in Biomedical Applications. *Advanced Materials* 25(16):2258-2268.
6. Shen H, Zhang L, Liu M, & Zhang Z (2012) Biomedical Applications of Graphene. *Theranostics* 2(3):283 -294.
7. Loh KP, Bao Q, Eda G, & Chhowalla M (2010) Graphene oxide as a chemically tunable platform for optical applications. *Nat Chem* 2(12):1015-1024.
8. Feng L & Liu Z (2011) Graphene in biomedicine: opportunities and challenges. *Nanomedicine* 6(2):317-324.
9. Ferrari AC*, et al.* (2006) Raman Spectrum of Graphene and Graphene Layers. *Physical Review Letters* 97(18):187401.
10. Bendali A*, et al.* (2013) Purified Neurons can Survive on Peptide-Free Graphene Layers. *Advanced Healthcare Materials*:929-933.
11. Liu Y, Dong X, & Chen P (2012) Biological and chemical sensors based on graphene materials. *Chemical Society Reviews* 41(6):2283-2307.
12. Seidlits SK, Lee JY, & Schmidt CE (2008) Nanostructured scaffolds for neural applications. *Nanomedicine (London, England)* 3(2):183-199.
13. Bianco A*, et al.* (2013) All in the graphene family – A recommended nomenclature for two-dimensional carbon materials. *Carbon* 65(0):1-6.
14. Wick P*, et al.* (2014) Classification Framework for Graphene-Based Materials. *Angewandte Chemie International Edition*:2-7.
15. Wilson NR*, et al.* (2009) Graphene Oxide: Structural Analysis and Application as a Highly Transparent Support for Electron Microscopy. *ACS Nano* 3(9):2547-2556.
16. Yang K*, et al.* (2011) In Vivo Pharmacokinetics, Long-Term Biodistribution, and Toxicology of PEGylated Graphene in Mice. *ACS Nano* 5(1):516-522.
17. Liu JH*, et al.* (2012) Effect of size and dose on the biodistribution of graphene oxide in mice. *Nanomedicine (London, England)* 7(12):1801-1812.
18. Zhan L*, et al.* (2011) Biodistribution of co-exposure to multi-walled carbon nanotubes and graphene oxide nanoplatelets radiotracers. *J Nanopart Res* 13(7):2939-2947.
19. Qu G*, et al.* (2013) The ex vivo and in vivo biological performances of graphene oxide and the impact of surfactant on graphene oxide's biocompatibility. *Journal of Environmental Sciences* 25(5):873-881.
20. Ali-Boucetta H*, et al.* (2012) Purified graphene oxide dispersions lack in vitro cytotoxicity and in vivo pathogenicity. *Adv Healthc Mater. 2013 Mar;2(3):433-41.*
21. Yang K*, et al.* (2013) In vivo biodistribution and toxicology of functionalized nano-graphene oxide in mice after oral and intraperitoneal administration. *Biomaterials* 34(11):2787-2795.
22. Yan L*, et al.* (2012) Can graphene oxide cause damage to eyesight? *Chem Res Toxicol* 25(6):1265-1270.
23. Zhang X*, et al.* (2011) Distribution and biocompatibility studies of graphene oxide in mice after intravenous administration. *Carbon* 49(3):986-995.
24. Duch MC*, et al.* (2011) Minimizing Oxidation and Stable Nanoscale Dispersion Improves the Biocompatibility of Graphene in the Lung. *Nano Letters* 11(12):5201-5207.
25. Schinwald A, Murphy FA, Jones A, MacNee W, & Donaldson K (2011) Graphene-Based Nanoplatelets: A New Risk to the Respiratory System as a Consequence of Their Unusual Aerodynamic Properties. *ACS Nano* 6(1):736-746.
26. Ma-Hock L*, et al.* (2013) Comparative inhalation toxicity of multi-wall carbon nanotubes, graphene, graphite nanoplatelets and low surface carbon black. *Part Fibre Toxicol* 10(1):23.
27. Girish CM, Sasidharan A, Gowd GS, Nair S, & Koyakutty M (2013) Confocal Raman Imaging Study Showing Macrophage Mediated Biodegradation of Graphene In Vivo. *Adv Healthc Mater* 2(10):1489-1500.

28. Bianco A (2013) Graphene: Safe or Toxic? The Two Faces of the Medal. *Angewandte Chemie International Edition* 52(19):4986-4997.
29. Kostarelos K & Novoselov KS (2014) Exploring the Interface of Graphene and Biology. *Science* 344(6181):261-263.
30. Bussy C, Jasim DA, Lozano N, Terry D, & Kostarelos K (2015) The Current Graphene Safety Landscape - a Literature Mining Exercise. *Nanoscale*.
31. Al-Jamal KT*, et al.* (2012) Degree of Chemical Functionalization of Carbon Nanotubes Determines Tissue Distribution and Excretion Profile. *Angewandte Chemie International Edition* 51(26):6389-6393.
32. Bussy C, Ali-Boucetta H, & Kostarelos K (2012) Safety Considerations for Graphene: Lessons Learnt from Carbon Nanotubes. *Accounts of Chemical Research* 46(3):692-701.
33. Dreyer DR, Park S, Bielawski CW, & Ruoff RS (2010) The chemistry of graphene oxide. *Chemical Society Reviews* 39(1):228-240.
34. Eigler S, Hu Y, Ishii Y, & Hirsch A (2013) Controlled functionalization of graphene oxide with sodium azide. *Nanoscale* 5(24):12136-12139.
35. Thomas HR, Marsden AJ, Walker M, Wilson NR, & Rourke JP (2014) Sulfur-Functionalized Graphene Oxide by Epoxide Ring-Opening. *Angew Chem Int Ed Engl* 4(10):1-7.
36. Kaiser E, Colescott RL, Bossinger CD, & Cook PI (1970) Color test for detection of free terminal amino groups in the solid-phase synthesis of peptides. *Analytical Biochemistry* 34(2):595-598.
37. Zhang W*, et al.* (2012) Unraveling Stress-Induced Toxicity Properties of Graphene Oxide and the Underlying Mechanism. *Advanced Materials* 24(39):5391-5397.
38. Zhang S, Yang K, Feng L, & Liu Z (2011) In vitro and in vivo behaviors of dextran functionalized graphene. *Carbon* 49(12):4040-4049.
39. Li Y*, et al.* (2013) Surface Coating-Dependent Cytotoxicity and Degradation of Graphene Derivatives: Towards the Design of Non-Toxic, Degradable Nano-Graphene. *Small*:1-11.
40. Szabó T, Berkesi O, & Dékány I (2005) DRIFT study of deuterium-exchanged graphite oxide. *Carbon* 43(15):3186-3189.
41. Jung I*, et al.* (2009) Reduction Kinetics of Graphene Oxide Determined by Electrical Transport Measurements and Temperature Programmed Desorption. *The Journal of Physical Chemistry C* 113(43):18480-18486.
42. Cornelissen B*, et al.* (2013) Nanographene oxide-based radioimmunoconstructs for in vivo targeting and SPECT imaging of HER2-positive tumors. *Biomaterials* 34(4):1146-1154.
43. Gómez-Navarro C*, et al.* (2010) Atomic Structure of Reduced Graphene Oxide. *Nano Letters* 10(4):1144-1148.
44. Yang K*, et al.* (2010) Graphene in Mice: Ultrahigh In Vivo Tumor Uptake and Efficient Photothermal Therapy. *Nano Letters* 10(9):3318-3323.
45. Lacerda L*, et al.* (2008) Dynamic Imaging of Functionalized Multi-Walled Carbon Nanotube Systemic Circulation and Urinary Excretion. *Advanced Materials* 20(2):225-230.
46. Ivanovskaya VV*, et al.* (2012) Graphene Edge Structures: Folding, Scrolling, Tubing, Rippling and Twisting. *GraphITA 2011* (Springer Berlin Heidelberg, Berlin), pp 75-85.
47. Meyer JC*, et al.* (2007) The structure of suspended graphene sheets. *Nature* 446(7131):60-63.
48. Patra N, Wang B, & Král P (2009) Nanodroplet Activated and Guided Folding of Graphene Nanostructures. *Nano Letters* 9(11):3766-3771.
49. Lacerda L*, et al.* (2008) Carbon-nanotube shape and individualization critical for renal excretion. *Small* 4(8):1130-1132.
50. Lacerda L*, et al.* (2012) Translocation mechanisms of chemically functionalised carbon nanotubes across plasma membranes. *Biomaterials* 33(11):3334-3343.
51. Russier J*, et al.* (2013) Evidencing a mask effect of graphene oxide: a comparative study on primary human and murine phagocytic cells. *Nanoscale*:11234-11247.
52. Singh R*, et al.* (2006) Tissue biodistribution and blood clearance rates of intravenously administered carbon nanotube radiotracers. *Proceedings of the National Academy of Sciences of the United States of America* 103(9):3357-3362.
53. Ruggiero A*, et al.* (2010) Paradoxical glomerular filtration of carbon nanotubes. *Proceedings of the National Academy of Sciences* 107(27):12369-12374.
54. Kostarelos K (2010) Carbon nanotubes: Fibrillar pharmacology. *Nature Materials* 9:793–795
55. Cagle DW, Kennel SJ, Mirzadeh S, Alford JM, & Wilson LJ (1999) In vivo studies of fullerene-based materials using endohedral metallofullerene radiotracers. *Proc Natl Acad Sci U S A* 96(9):5182-5187.

56. Yang K, *et al.* (2012) The influence of surface chemistry and size of nanoscale graphene oxide on photothermal therapy of cancer using ultra-low laser power. *Biomaterials* 33(7):2206-2214.
57. Hong H, *et al.* (2012) In vivo targeting and positron emission tomography imaging of tumor vasculature with (66)Ga-labeled nano-graphene. *Biomaterials* 33(16):4147-4156.
58. Hong H, *et al.* (2012) In Vivo Targeting and Imaging of Tumor Vasculature with Radiolabeled, Antibody-Conjugated Nanographene. *ACS Nano* 6(3):2361-2370.
59. Wang K, *et al.* (2011) Biocompatibility of graphene oxide. *Nanoscale Res Lett* 6(8):1-8.
60. Singh SK, *et al.* (2011) Thrombus Inducing Property of Atomically Thin Graphene Oxide Sheets. *ACS Nano* 5(6):4987-4996.
61. Ralph W, Matthias N, & Mikael JP (2014) Imaging macrophages with nanoparticles. *Nature Materials* 13(2):125-138.
62. Patil RR, Gaikwad RV, Samad A, & Devarajan PV (2008) Role of Lipids in Enhancing Splenic Uptake of Polymer-Lipid (LIPOMER) Nanoparticles. *Journal of Biomedical Nanotechnology* 4(3):359-366.
63. Ménard-Moyon C, Fabbro C, Prato M, & Bianco A (2011) One-Pot Triple Functionalization of Carbon Nanotubes. *Chemistry – A European Journal* 17(11):3222-3227.

Figure Legends

Scheme 1: Preparation of GO-DOTA by a two-step derivatization method. For the sake of clarity, only one epoxide group is derivatized.

Figure 1: (A) Structural characterization of GO (i) and GO-DOTA (ii) by TEM (left), AFM and AFM-height section (right). (B) Physicochemical characterization using (i) FT-IR spectroscopy of GO, GO-NH_2, GO-DOTA, TEG diamine, and DOTA-NCS; (ii) XPS N (1s) peak of GO-NH_2 and GO-DOTA; (iii) TGA of GO, GO-NH_2, GO-DOTA, TEG diamine, and DOTA-NCS under inert atmosphere; (iv) Raman spectroscopy of graphite, GO, and GO-DOTA, with corresponding I_D/I_G ratio.

Figure 2: (A) Whole body Nano-SPECT/CT imaging of a C57BL/6 mouse injected with 50 µg of GO-DOTA[^{111}In], imaged at different time points (1, 4, and 24 h), showing from left to right whole body, sagittal, coronal and transverse views. (B) Major organ biodistribution, (C) blood profile, and (D) levels of radioactivity detected in urine and faeces after 24 h detected by gamma scintigraphy. Statistical significance was * < 0.05 against both controls using Student's t-test. Four different mice were used per group.

Figure 3: Translocation events in mice injected with 50 µg of GO-DOTA chelated with non-radioactive $InCl_3$ after 1 and 24 h. (A) Liver and (B) spleen examinations using (i) H&E staining and (ii) Raman spectroscopy (average of 3 spectra) (left) and corresponding optical micrographs (right). All scale bars are 50 µm.

Figure 4: Detection of GO-DOTA in the urine of injected C57BL/6 mice 24 h post-injection as shown by: (A) Raman spectroscopy showing the GO signatures obtained from different spots within the urine sample (orange curves) and the corresponding dark-field micrographs of the samples (right). (B) HR-TEM of GO-DOTA found in the urine (i) and corresponding SAED diffraction pattern (ii, iii). Another HR-TEM image of GO-DOTA found in the urine (iv) and zoom-in images showing ordered areas (v, vi, vii).

Supporting Information

Tissue Distribution and Urinary Excretion of Intravenously Administered Chemically Functionalized Graphene Oxide Sheets

Dhifaf A. Jasim, Cécilia Ménard-Moyon, Dominique Bégin, Alberto Bianco, Kostas Kostarelos**

Supporting Figures

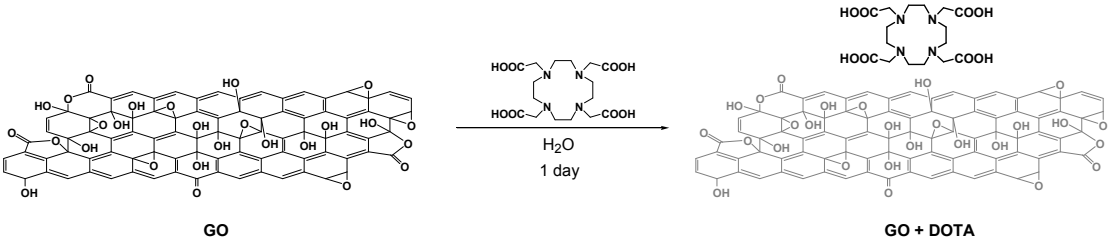

Scheme S1: Preparation of control sample GO + DOTA. GO was simply mixed with DOTA and treated to remove excess DOTA which was not physically adsorbed onto GO.

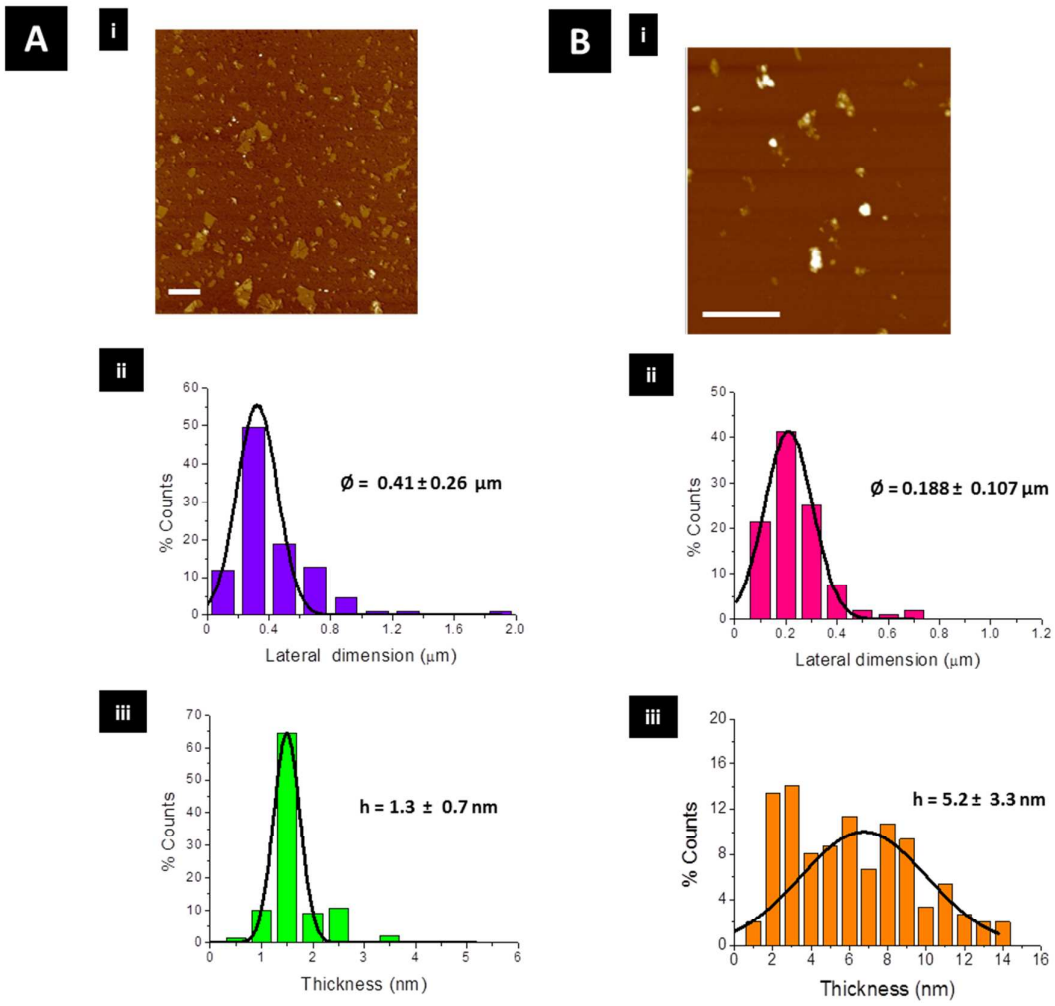

Supporting Figure 1: AFM of (A) GO and (B) GO-DOTA. (i) AFM images; (ii) lateral size distribution measured by counting the lateral dimension; (iii) thickness distribution obtained from height sections. Percent counts were obtained by counting more than 100 sheets obtained from several images per sample. Scale bars are 1µm.

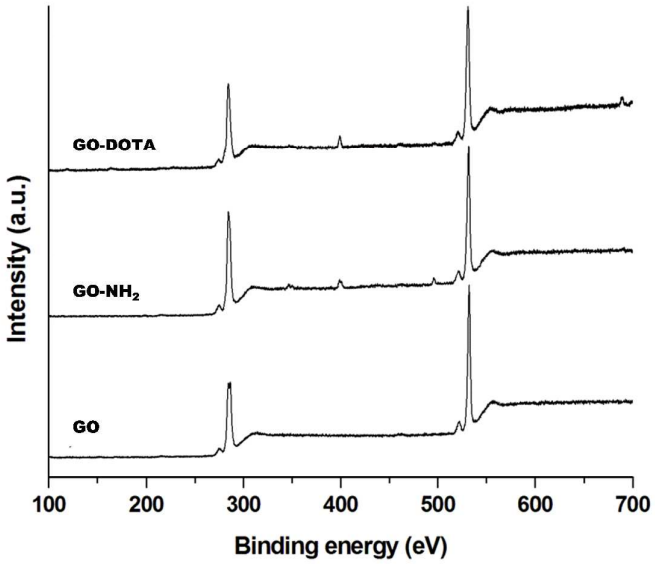

Supporting Figure 2: XPS of GO, GO-NH_2 and GO-DOTA showing the appearance of the N (1s) peak at ~400 eV, compared to XPS of GO.

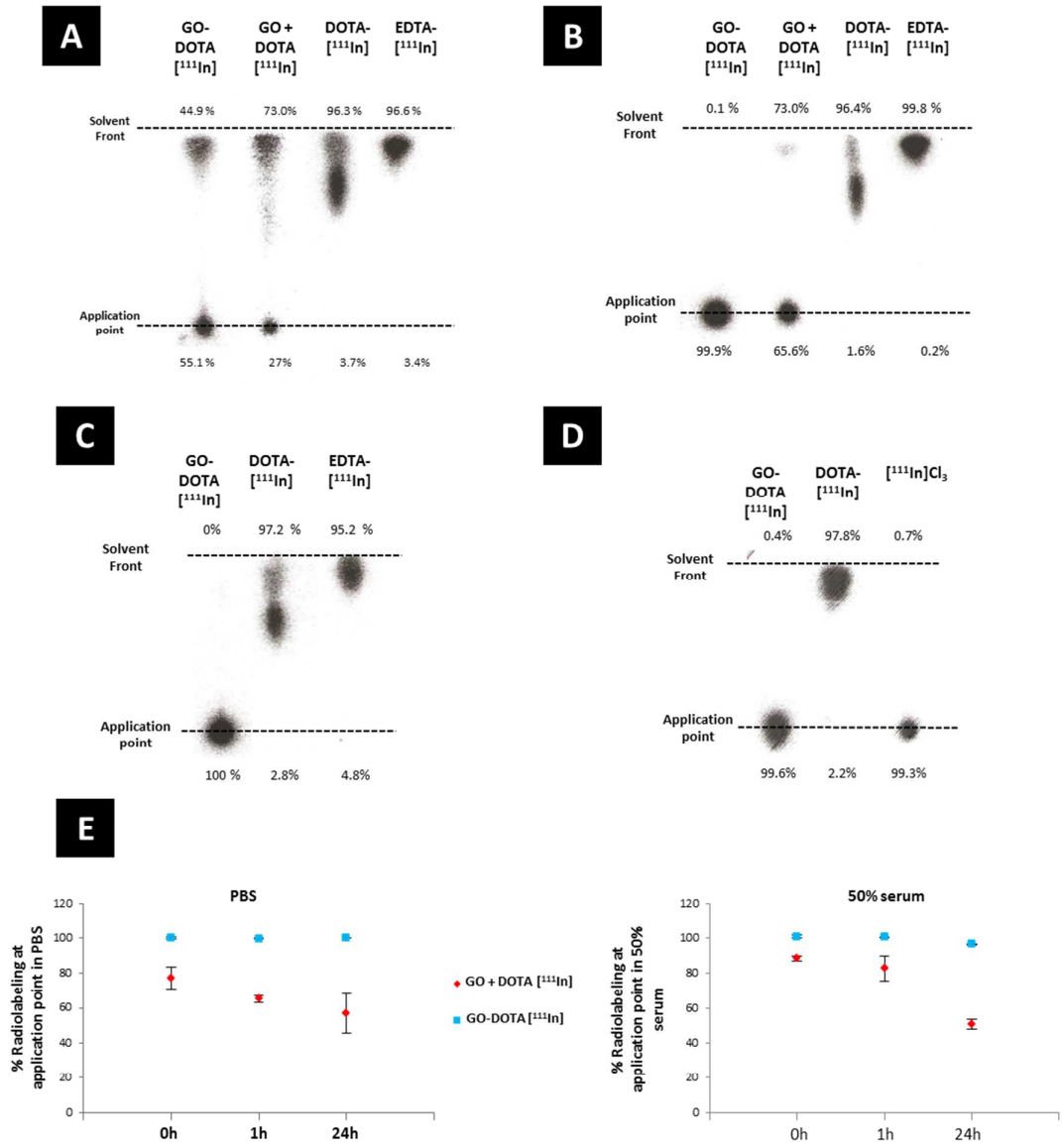

Supporting Figure 3: Thin layer chromatography of radiolabeled constructs showing: (A) labeling efficiency after radiolabeling with ^{111}In of the chemically conjugated (GO-DOTA) compared to the physically adsorbed control (GO + DOTA); (B) removal of free ^{111}In from GO-DOTA[^{111}In] sample by centrifugation for 30 min compared to the physically adsorbed control (GO + DOTA[^{111}In]); (C) no free (unbound) ^{111}In was detected before injecting samples in mice; (D) DOTA conjugation efficiency detected by using a modified running buffer at pH 9; (E) radiolabeling stability up to 24h of the chemically conjugated sample (GO-DOTA[^{111}In]) compared to the physically adsorbed control (GO + DOTA[^{111}In]) at 37°C, in both 50% serum and PBS.

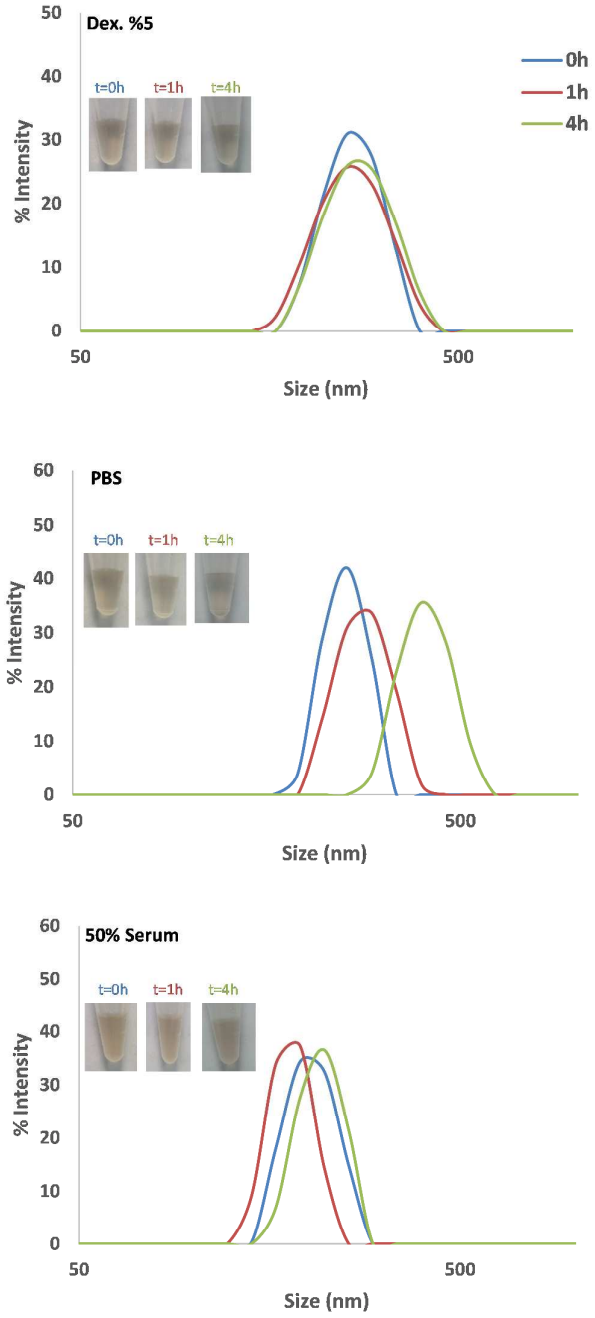

Supporting Figure 4: Colloidal stability of the GO-DOTA sheets dispersed in Dextrose, PBS and serum (50%) (from top to bottom) for t=0, 1h and 4h. The mean size of the dispersed material was measured using dynamic light scattering using Malvern Zetasizer Nano ZS (UK).

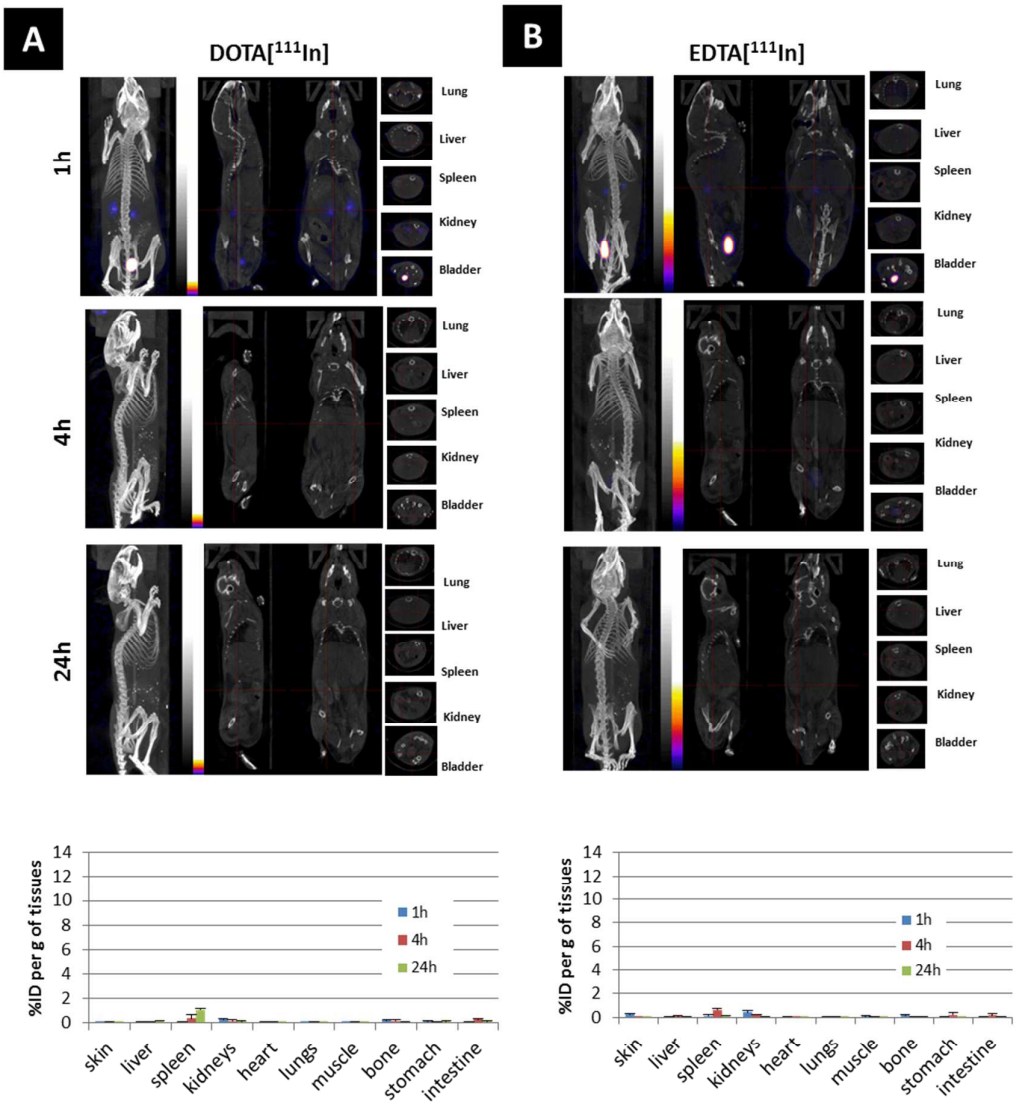

Supporting Figure 5: Biodistribution of **(A)** DOTA[^{111}In] and **(B)** EDTA[^{111}In]. Whole body SPECT/CT imaging of a C57BL/6 mouse injected with DOTA[^{111}In] and EDTA[^{111}In], respectively, imaged at different time points (1, 4, 24 h) showing from left to right whole body, sagittal, coronal and transverse views. Gamma scintigraphy bar charts showing organ biodistribution (n=4/group).

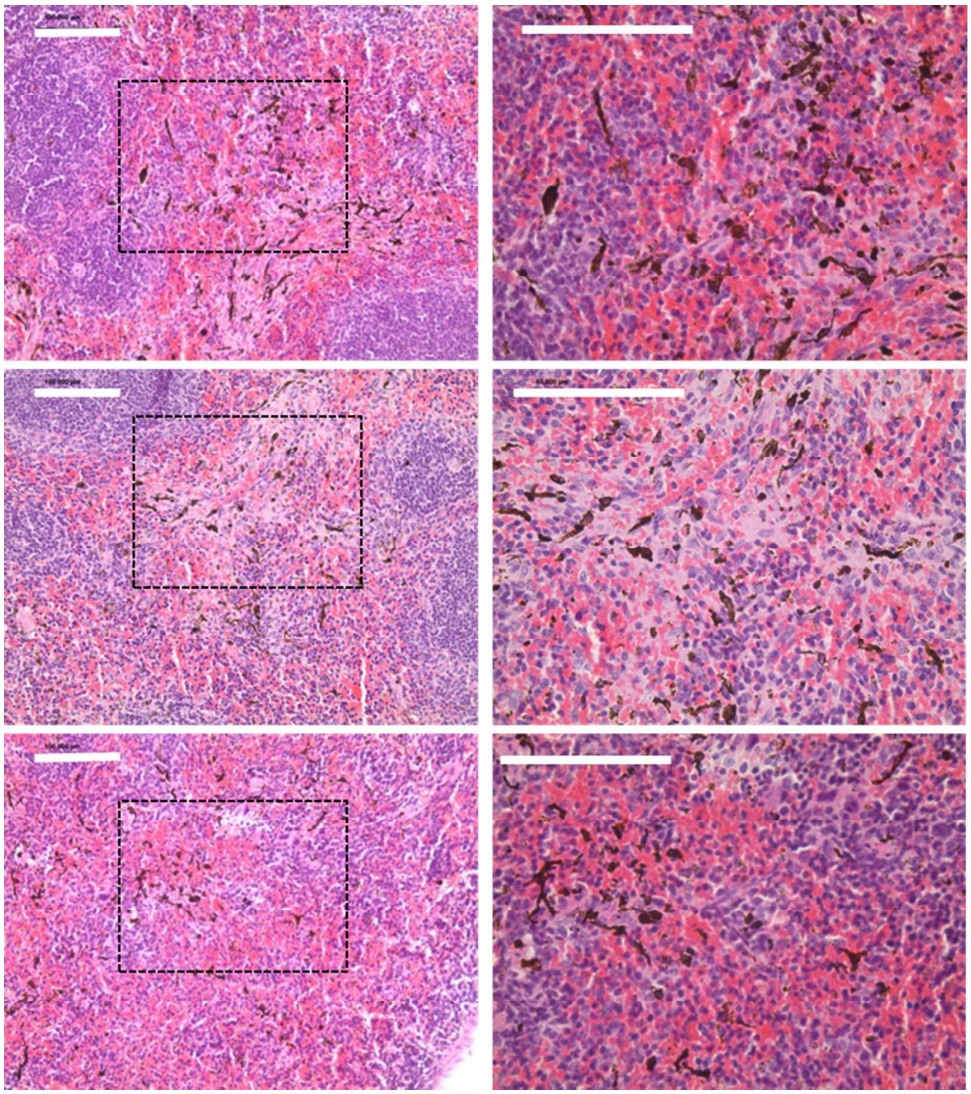

Supporting Figure 6: Histology using H & E staining of spleen sections showing GO-DOTA accumulation at 24h post-injection. Right hand-side images are higher magnification images of the boxes on the left hand-side sections. All scale bars are 100 μm.

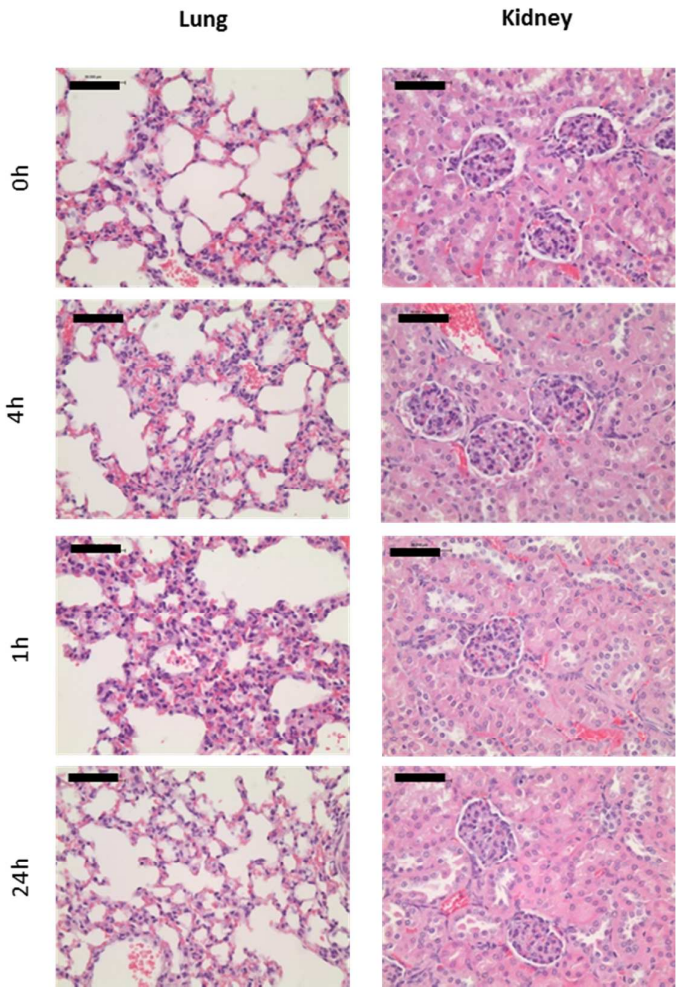

Supporting Figure 7: Histology using H & E staining of lung (left) and kidney (right) tissue sections from mice injected with 50 µg of GO-DOTA chelated with non-radioactive $InCl_3$ after 1, 4 and 24h compared to uninjected mice at time 0h. All scale bars are 50 µm.

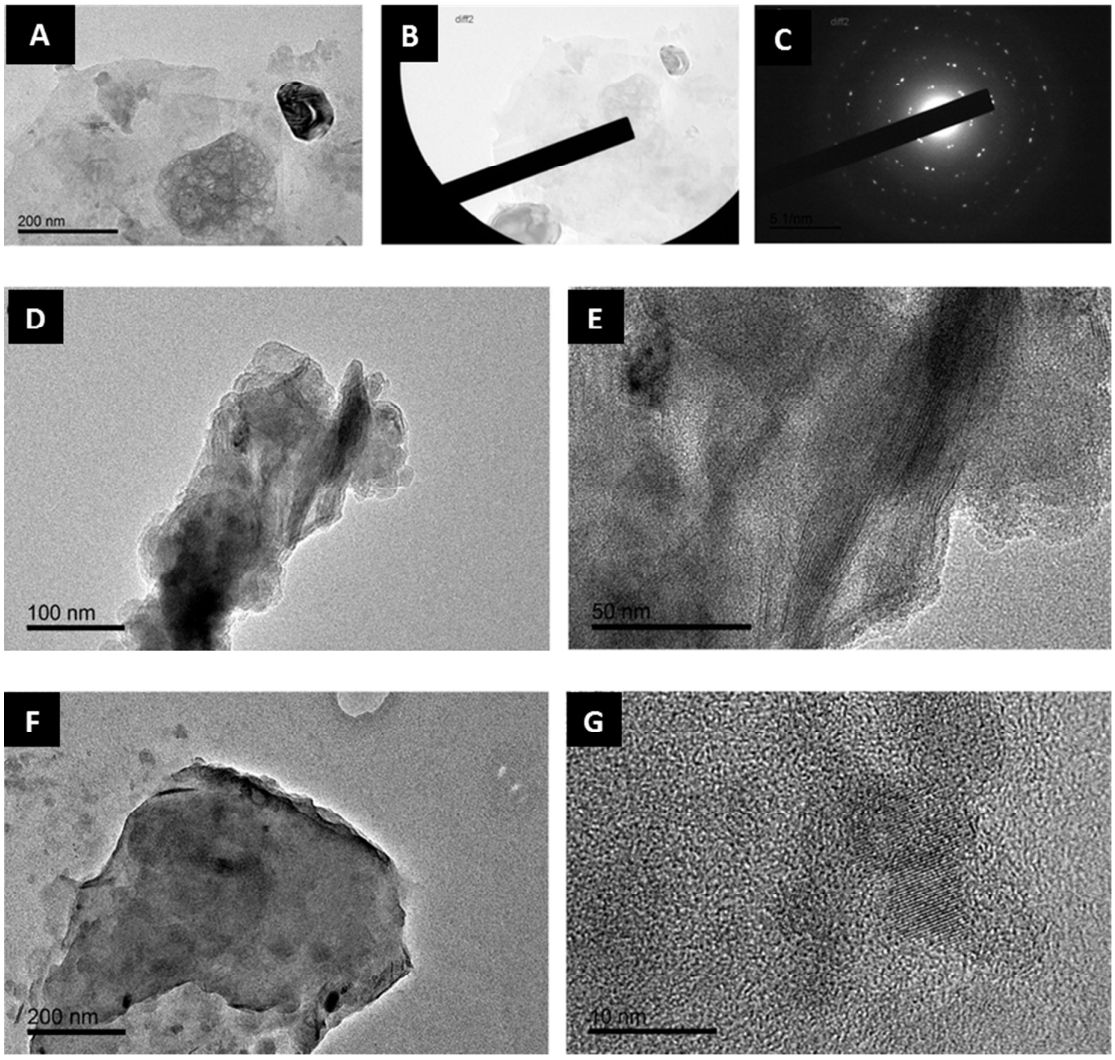

Supporting Figure 8: HR-TEM of GO-DOTA found in the urine after 24h **(A)** and their corresponding SAED diffraction patterns **(B, C)**. Other HR-TEM images of GO-DOTA found in the urine **(D, E)** and corresponding magnification images showing ordered areas **(F, G)**.